

Thermodynamic behaviour of magnetocaloric quantities in spin-1/2 Ising square trilayer

Soham Chandra[†] and Mukdish Acharyya^{*}

Department of Physics, Presidency University

86/1 College Street, Calcutta-700073, India

E-mail: [†]soham.rs@presiuniv.ac.in; ^{*}muktish.physics@presiuniv.ac.in

Abstract

We have studied a spin-1/2, Ising trilayered ferrimagnetic system on square Bravais lattice, employing Monte-Carlo simulation with single spin-flip Metropolis algorithm. The bulk of such a system is formed by three layers, each of which is composed completely either by A or B type of atoms, resulting in two distinct compositions: ABA and AAB and two different types of magnetic interactions: ferromagnetic between like atoms and antiferromagnetic between unlike atoms. Variation of relative interaction strengths in the Hamiltonian, for a range of values, leads to the shift of compensation point and critical point and changes in the magnitude of reduced residual magnetisation. We have tried to put forward probable mathematical forms of dependences of the reduced residual magnetisation and temperature interval between the compensation and critical points on controlling parameters in absence of applied magnetic field and have obtained phase diagrams for both types of configurations from these relations.

Keywords: Ising trilayer, Metropolis algorithm, residual magnetisation, compensation temperature, critical temperature

I. Introduction

Ferrimagnetism was discovered in 1948 [1]. In the past decades, studies on ferrimagnets have revealed unique properties, showing their potential in technological applications like magneto-optical devices [2, 3], Giant magnetoresistance (GMR) [4], Magnetocaloric effect (MCE) [5, 6]. A ferrimagnet is modelled as a combination of two or more magnetic substructures, like, subsets of atoms, sublattices, or layers. Layered ferrimagnetic materials present characteristics, quite different from the bulk. Owing to their enhanced surface-to-volume ratio, the surface atoms may provide significant contributions to the physical properties of the system, as a whole. With the advent of different thin film growth techniques, like, molecular-beam epitaxy (MBE) [7], atomic layer deposition (ALD) [8], metalorganic chemical vapor deposition (MOCVD) [9], pulsed laser deposition (PLD) [10], experimental growth of bilayered [11], trilayered [12], and multilayered [13, 14] systems with desired characteristics has been achieved. This is one of the reasons behind increased interest in the theoretical and experimental studies of magnetic properties of layered magnets.

For a layered ferrimagnet, each of the layers may have different thermal dependencies for magnetization. Such different behaviours, when combined together, may show some interesting phenomenon such as *compensation*, i.e., there exists temperature below the critical point, called **compensation point**, for which total magnetization of the bulk vanishes while individual layers have magnetic order [1]. Compensation is not related to criticality of the system but physical properties like the magnetic coercivity exhibits singular behavior at the compensation point [2, 3]. Compensation point of some ferrimagnetic materials at room temperature and strong temperature dependence of coercive field around compensation point, makes these materials particularly useful for thermomagnetic recording devices [2]. In 2D Ising planar ferrimagnets, compensation occurs in mixed-spin cases with combinations of different spins [15, 16, 17]. For layered single-spin systems having even number of layers, necessity of site dilution and strict restrictions on the conditions of controlling parameters for the occurrence of compensation effect has been verified through pair approximation (PA) calculations [18, 19, 20] for the Ising-Heisenberg systems and by MC simulations for the Ising systems [21, 22]. But for odd number of layers, neither site dilution [23] nor mixed-spin cases [24, 25] are necessary for observing compensation. That is why our area of interest in this article is compensation point, T_{comp} , of the trilayered spin-1/2 Ising ferrimagnet. For being a single-spin model, such systems are, computationally and growth wise, less expensive than other ferrimagnetic models and belongs to the simplest of spin-systems for compensation. In literature, using Ising mechanics, layered systems have been studied by equilibrium Monte Carlo (MC) simulations in [26, 27], by mean-field approximation (MFA) in [28], by effective-field approximation (EFA) in [29, 30, 31, 32], by series-expansion method in [33], by renormalization-group (RG) method in [34], by spin-fluctuation theory in [35], by exact recursion equation on the Bethe lattice in [36] and by cluster variation method in pair approximation in [37].

Magnetocaloric effect (MCE) is defined by heating or cooling of a magnetic material, with the variation of applied magnetic field making it a good candidate for new type of refrigerant materials for construction of energy efficient devices and that is why its potential is thoroughly investigated in [38, 39]. After the discovery of MCE in iron by Warburg in 1881 [40], theoretical explanations were provided by Debye in 1926 [41] and Giauque in 1927 [42]. MCE is characterized by the magnetic entropy change, ΔS and/or adiabatic temperature change, ΔT and we have Maxwell's relation $\left(\frac{\partial S}{\partial H}\right)_T = \left(\frac{\partial M}{\partial T}\right)_H$ connecting them, with H and T being applied magnetic field and temperature of the system. This relation shows, for an abrupt change of magnetization around the compensation point, for most of the ferrimagnets with compensation, we may expect large MCE. For the first-order phase transitions, large changes in entropy, usually are observed in the neighbourhood of transition due to sharp change in magnetization [43, 44]. But such materials suffer from hysteretic behavior and a narrow range of working temperature, as a magnetic refrigerant [45]. But, second-order transition materials, because of absence of magnetic and thermal hysteresis and wide interval of transition temperatures, are extensively studied [46] and at present most of them are operated near their transition temperatures for magnetic refrigeration. In layered ferrimagnets, especially with odd number of layers, we witness a sharp change in magnetization across compensation point. Thus such materials have an advantage over conventional second order magnetic transition materials, in having a lower temperature than critical point with high value of ΔM . But such ferrimagnetic materials, have not been studied widely as magnetocaloric materials yet.

Because of a limited number of exact methods available, approximate and numerical studies have their own importance. Referring to recent studies on compensation in the literature, it is reported, by MFA and EFA in [24] and by MC simulations with Single cluster Wolff Algorithm in [25] that under certain range of different types of interaction strengths between lattice sites, different temperature dependencies of sublattice magnetisations cause the compensation point to appear in an Ising trilayer on square lattice. A quasi three-dimensional, spin-1/2, Ising trilayer stacking on square lattice with quenched non-magnetic impurity is studied in [47] and it is observed, the critical and compensation points, can be modulated to drift towards lower temperatures with increasing concentration of non-magnetic impurities and in [48], it was hinted that reduced residual magnetisation, another magnetocaloric quantity, possibly varies in a systematic way. In [49], the dilution effects on compensation temperature in nanotrilinear graphene structure were studied through MC simulation and it has been found that with reduction in dilution probability, compensation temperature, *increases* in an ABA system and *decreases* in BAB systems. In [50], by the MC approach, the appearance of two compensation temperatures is reported in a mixed spin (7/2, 1) antiferromagnetic ovalene nanostructures. It was observed by MC simulation [51], in Blume Capel model of a bilayer graphene structure with Ruderman-Kittel-Kasuya-Yosida (RKKY) interactions, the transition temperature increases with decrease in the number of nonmagnetic layers. Dilution effects on compensation temperature in borophene core-shell structure is studied in [52] by MC simulations the magnetic properties of a diluted core-shell borophene structure are studied and

the existence of the compensation and transition temperatures for special physical parameters and hysteresis cycles are analyzed. The trilayered Blume-Capel ($S = 1$) magnet is studied in [53] by Monte Carlo simulation and the equilibrium behaviours of critical and compensation temperatures and the dependence of these two temperature on the anisotropy are reported and comprehensive phase diagrams in Hamiltonian parameter space are drawn. We introduce Reduced residual magnetisation (RRM) as the absolute value of the ratio of the peak value of the magnetisation in between compensation and critical points and the saturated value of magnetisation and observe its variation against controlling parameters. Our objective is to find possible mathematical forms of dependences of various magnetocaloric quantities on the controlling parameters namely relative interaction strengths which might be helpful for experimentalists in designing a material for their desired magnetocaloric characteristics.

The formation of this article is as follows. Microscopic structure and the Ising Hamiltonian for the trilayer system is in Section II. Details of the MC simulation scheme and the calculated quantities are in Section III. Numerical results are in Section IV. Next, in Section V, there are concluding remarks and summary of the article is in Section VI.

II. Model

We consider, in this study, an Ising superlattice containing three magnetic layers on square lattice with the following details (as in [24, 25]):

- (a) Each layer is exhaustively composed by either of the two possible types of atoms, A or B with coordination number being 6 or 5 depending on that site being on the mid-layer or on the surface layers.
- (b) Three different interactions of two types, between atoms, exist:
 - A-A \rightarrow Ferromagnetic
 - B-B \rightarrow Ferromagnetic
 - A-B \rightarrow Anti-ferromagnetic
- (c) Two distinct stackings are possible: (i) AAB [Fig.-1a] and (ii) ABA [Fig.-1b].

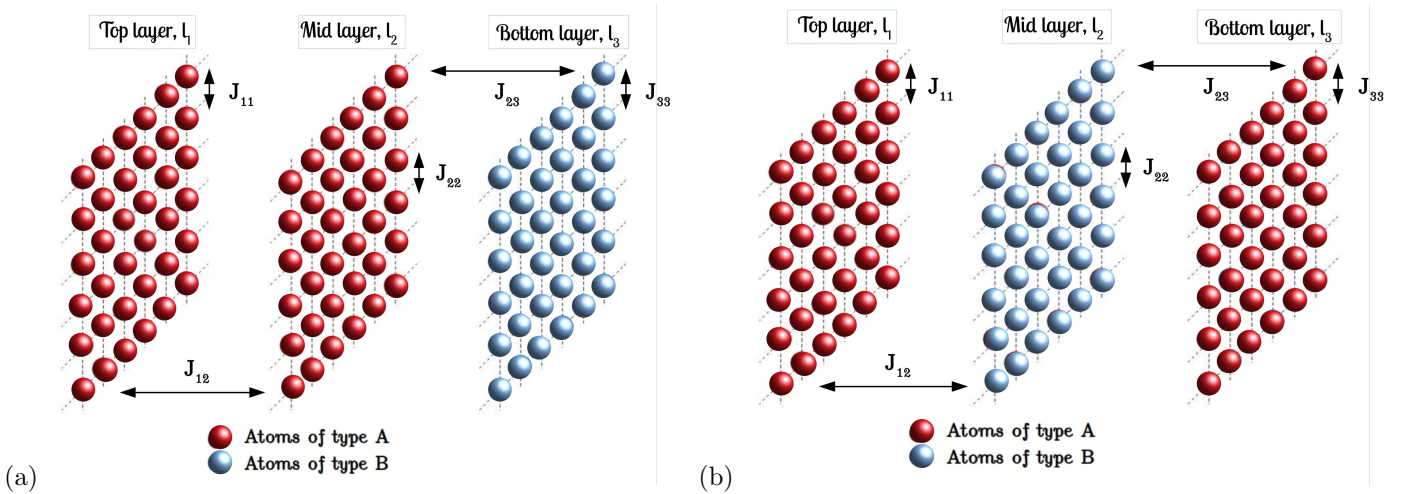


Figure 1: Two distinct trilayer stackings: (a) AAB stacking (with $J_{11} = J_{22} = J_{12} = J_{AA}$, $J_{33} = J_{BB}$ and $J_{23} = J_{AB}$) (b) ABA stacking (with $J_{11} = J_{33} = J_{AA}$, $J_{22} = J_{BB}$ and $J_{12} = J_{23} = J_{AB}$).

The equilibrium spin configuration on any layer is determined by the condition that the free energy of the whole system should be a minimum. As we've considered the spins to interact Ising-like, in-plane as well as out-of-plane, the Hamiltonian for the trilayer system is:

$$H = -J_{11} \sum_{\langle t, t' \rangle} S_t S_{t'} - J_{22} \sum_{\langle m, m' \rangle} S_m S_{m'} - J_{33} \sum_{\langle b, b' \rangle} S_b S_{b'} - J_{12} \sum_{\langle t, m \rangle} S_t S_m - J_{23} \sum_{\langle m, b \rangle} S_m S_b \quad (1)$$

where $\langle t, t' \rangle$, $\langle m, m' \rangle$, $\langle b, b' \rangle$ are, respectively, summations over all nearest-neighbor pairs in the top, mid and bottom layers and $\langle t, m \rangle$, $\langle m, b \rangle$ are, respectively, summations over pairs of nearest-neighbor sites in adjacent layers, top & mid and mid & bottom layers. In Equation [1], the first, second and third terms respectively are for the intra-planar contributions from the top-layer, mid-layer and bottom-layer. The fourth and the fifth terms arise out of the nearest neighbour inter-planar interactions, between top and mid layers and mid and bottom layers.

For the AAB type trilayer system, the nature of the coupling strengths in Equation [1] are: $J_{11} > 0$, $J_{22} > 0$, $J_{33} > 0$ and $J_{12} > 0$, $J_{23} < 0$ and we call $J_{11} = J_{22} = J_{12} = J_{AA}$, $J_{33} = J_{BB}$ and $J_{23} = J_{AB}$. But when we switch to ABA type system, we have in Equation [1]: $J_{11} > 0$, $J_{22} > 0$, $J_{33} > 0$ and $J_{12} < 0$, $J_{23} < 0$

and we call $J_{11} = J_{33} = J_{AA}$, $J_{22} = J_{BB}$ and $J_{12} = J_{23} = J_{AB}$. We've considered periodic boundary conditions in-plane and open boundary conditions along the vertical, so that there is no out-of-plane interaction term between the top and bottom layer in the Hamiltonian.

III. Simulation Scheme

The model described above was simulated using the Monte Carlo simulations with Metropolis single spin-flip algorithm [54, 55] with each plane having L^2 sites with a system size having $L = 100$. For $L \geq 60$ compensation point tends to a stable value [25], thus the lattice size in our study is quite standard. The initial high temperature paramagnetic phase of spin configurations had randomly selected 50% of total number of spins in upward projection with $S_i = +1$ and the rest in downward projection with $S_i = -1$ (Using 1 instead of 1/2 rescales the coupling constants only). At a fixed temperature T , spin flipping from S_i to $-S_i$ was done by using the Metropolis rate [56, 57]:

$$P(S_i \rightarrow -S_i) = \min\{1, \exp(-\Delta E/k_B T)\} \quad (2)$$

where ΔE is the change in internal energy due to the change of the orientation of the i -th spin projection from S_i to $-S_i$ with Boltzmann constant, k_B set to 1. Similar $3L^2$ random updates of spins constitute one Monte Carlo sweep (MCS) of the entire system and define one unit of time in our study. At each temperature step, starting from the configuration of previous temperature, the system was equilibrated till 5×10^4 MCS (that is equivalent to allowance of a long enough *time*) and thermal averages were calculated from further 5×10^4 MCS, i.e. we take total MCS, $N = 10^5$. We observed the system for ten values of J_{AA}/J_{BB} , starting from 0.1 to 1.0 and for each fixed value of J_{AA}/J_{BB} , we varied J_{AB}/J_{BB} from -0.1 to -1.0 with an interval of -0.1 . For each of the values of J_{AA}/J_{BB} and J_{AB}/J_{BB} , we've calculated the time (or, ensemble) averages of the following quantities at each of the temperature points, in the following manner:

(1) **Sublattice magnetisations** for top, mid and bottom layers calculated, identically, at say, i -th MCS after equilibration, denoted by M_{qi} , by:

$$M_{qi} = \frac{1}{L^2} \sum_{x,y=1}^L (S_{qi})_{xy} \quad (3)$$

and the sum extends over all sites in each of the planes as x and y denote the co-ordinates of a spin on a plane and runs from 1 to L (which is 100, in our study). Then we get the time (or, ensemble) average, from the last $N/2$ MCS, as follows:

$$\langle M_q \rangle = \frac{2}{N} \sum_{i=\frac{N}{2}+1}^N M_{qi} \quad (4)$$

where q is to be replaced by t, m or b for top, mid and bottom layers and $\langle \dots \rangle$ denotes a time average (equivalently ensemble average) after attaining equilibrium.

(2) Time average value of **Average magnetisation of the trilayer** by $\langle M \rangle = \frac{1}{3} (\langle M_t \rangle + \langle M_m \rangle + \langle M_b \rangle)$

(3) After attaining equilibrium, we calculate **fluctuation in magnetisation**, ΔM from the final $N/2$ MCS as follows:

$$\Delta M = \sqrt{\frac{2}{N-2} \sum_{i=\frac{N}{2}+1}^N (M_i - \overline{M})^2} \quad (5)$$

where M_i is the value of magnetisation of the whole system, calculated after the completion of i -th MCS and \overline{M} is the average value of total magnetisation calculated over the $N/2$ MCS after equilibration. We store all the obtained values and then make sample averages (over 10 statistically independent microscopic samples with same macroscopic initial conditions) to report the values of these quantities for further investigation.

IV. Results and Discussion

From the plot of Fig.-2a, We first note the presence of compensation, and note coordinates of immediate neighbouring points on both sides of zero line to find out the value of compensation point by the method of linear interpolation. Then, we find out the value of *reduced residual magnetisation* by calculating the absolute value of the ratio between intermediate maximum/minimum value of magnetization between critical and compensation temperature and the saturated value of magnetization, which is a dimensionless quantity.

From the plot of Fig.-2b, We note the value of temperature where the fluctuation in magnetization reaches its maximum value, and quote that temperature as the critical temperature, and subsequently obtain the difference between critical and compensation temperatures. After that we fit the obtained data so far to get the possible functional forms for these two quantities. All the while we would be working with best values of underlying quantities to qualitatively figure out mathematical dependences.

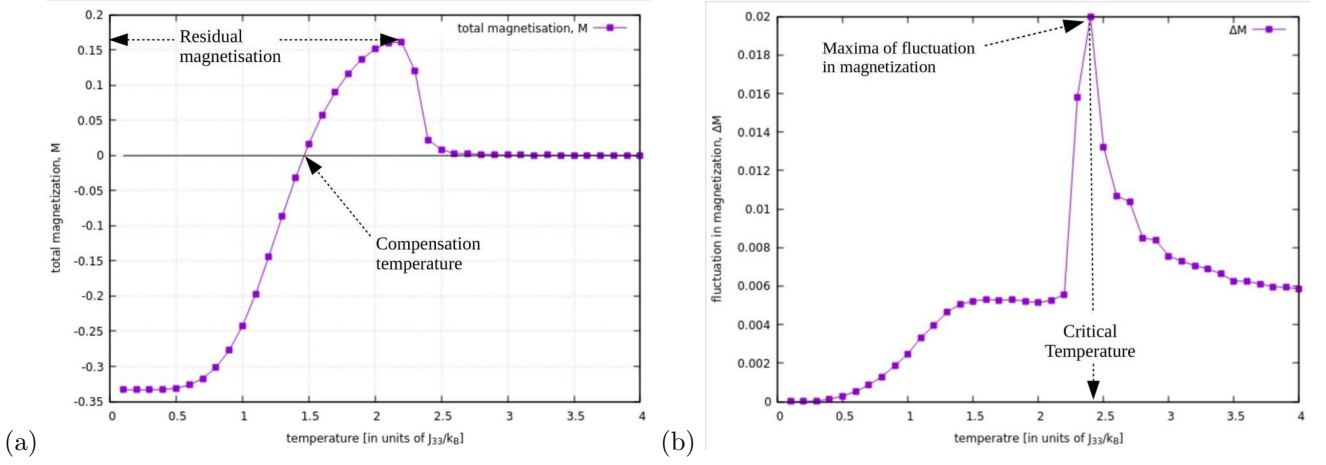


Figure 2: The plots of AAB configuration of (a) total magnetisation vs. temperature and (b) fluctuation in magnetization vs. temperature [for $J_{AA}/J_{BB} = 0.3$ and $J_{AB}/J_{BB} = -0.4$] show how observed quantities are extracted

a. Morphology

The density plots of the spin matrices of three layers, in the presence of compensation effect for both the configurations, show that the critical temperature and the compensation temperature are morphologically different.

At T_{comp} , due to the configuration of AAB system, compensation happens for satisfying the following conditions (which can readily be verified from Fig.-3, Fig.-4 & Fig.-5):

$$|M_b| = |M_t + M_m| \quad (6)$$

$$\text{sgn}(M_b) = -\text{sgn}(M_t) \quad (7)$$

$$\text{sgn}(M_b) = -\text{sgn}(M_m) \quad (8)$$

Fig.-3, Fig.-4 and Fig.-5 are spin density matrix plots for AAB system with $J_{AA}/J_{BB} = 0.3$ and $J_{AB}/J_{BB} = -0.4$. For such a configuration, the bottom-layer, b , is antiferromagnetically coupled to the mid-layer, m and thus magnetically saturates in the opposite direction to both, t and m . At T_{crit} , larger spin clusters results in bottom layer having greater absolute value of magnetisation than the top and mid layer.

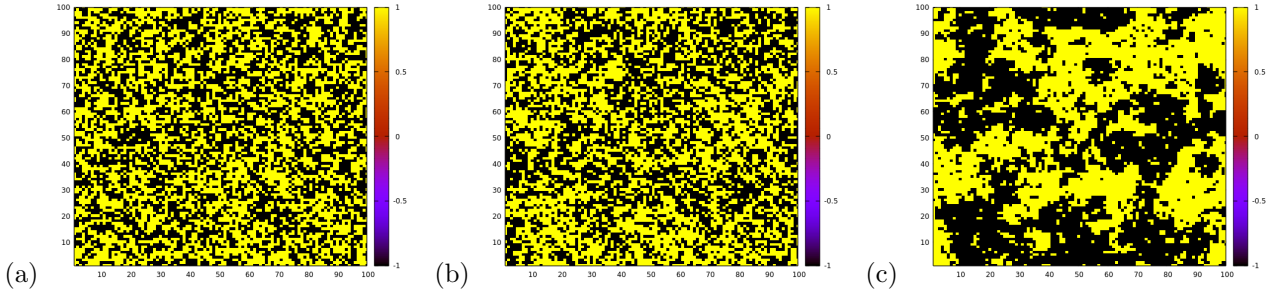


Figure 3: Morphology of (a) Top layer, (b) Mid layer and (c) Bottom layer for the AAB stacking ($J_{AA}/J_{BB} = 0.3$ and $J_{AB}/J_{BB} = -0.4$) at $T_{crit} = 2.4$ with $M_t = -0.01$, $M_m = -0.05$, $M_b = 0.17$.

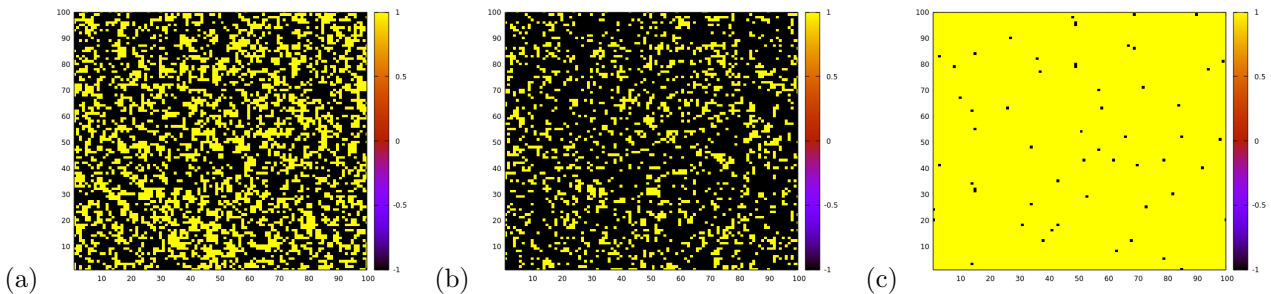


Figure 4: Morphology of (a) Top layer, (b) Mid layer and (c) Bottom layer for the AAB stacking ($J_{AA}/J_{BB} = 0.3$ and $J_{AB}/J_{BB} = -0.4$) at $T = 1.5$ (immediate higher neighbour than T_{comp}) with $M_t = -0.32$, $M_m = -0.62$, $M_b = 0.99$.

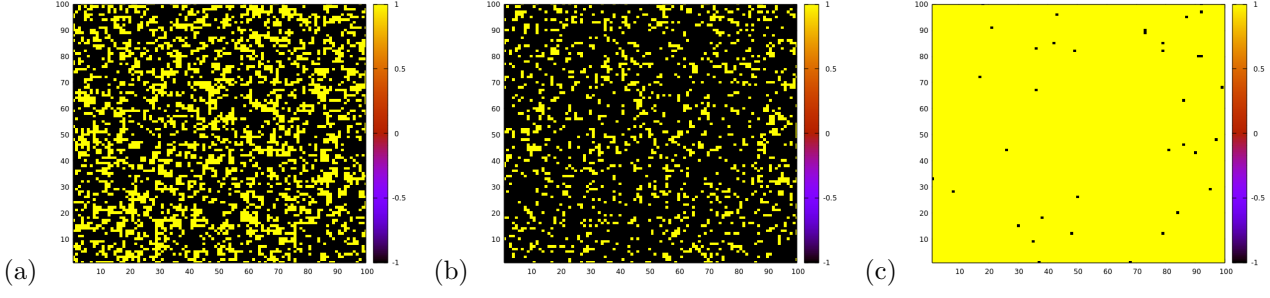


Figure 5: Morphology of (a) Top layer, (b) Mid layer and (c) Bottom layer for the AAB stacking ($J_{AA}/J_{BB} = 0.3$ and $J_{AB}/J_{BB} = -0.4$) at $T = 1.4$ (immediate lower neighbour than T_{comp}) with $M_t = -0.39$, $M_m = -0.69$, $M_b = 0.99$.

Similarly for ABA type systems, the conditions for compensation change to the following:

$$|M_m| = |M_t + M_b| \quad (9)$$

$$\text{sgn}(M_m) = -\text{sgn}(M_t) \quad (10)$$

$$\text{sgn}(M_m) = -\text{sgn}(M_b) \quad (11)$$

Fig.-6, Fig.-7, Fig.-8 are spin density matrix plots for ABA system with $J_{AA}/J_{BB} = 0.3$ and $J_{AB}/J_{BB} = -0.4$. As the mid-layer, m , is antiferromagnetically coupled to both the t and b layers, mid-layer always magnetically saturates in the opposite direction to both, t and b layers for an ABA system. At T_{crit} , it is seen that larger spin clusters form in the mid layer resulting in its having greater absolute value of magnetisation than the top and bottom layer.

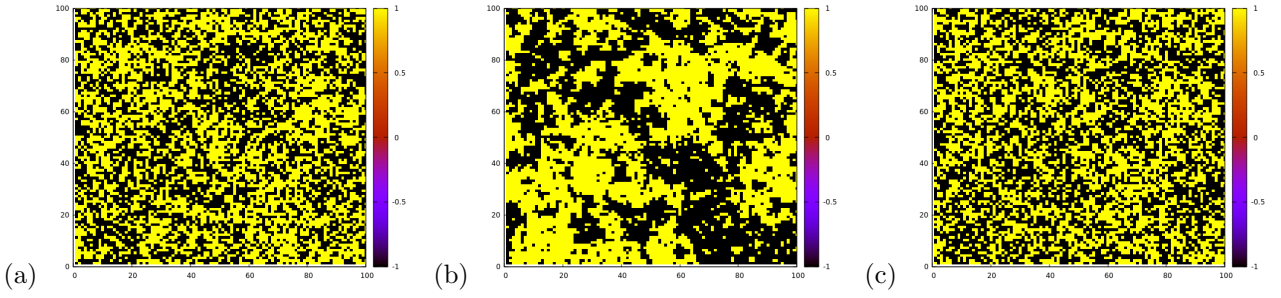


Figure 6: Morphology of (a) Top layer, (b) Mid layer and (c) Bottom layer for the ABA stacking ($J_{AA}/J_{BB} = 0.3$ and $J_{AB}/J_{BB} = -0.4$) at $T_{crit} = 2.6$ with $M_t = -2.91 \times 10^{-3}$, $M_m = 1.23 \times 10^{-2}$, $M_b = -3.07 \times 10^{-3}$.

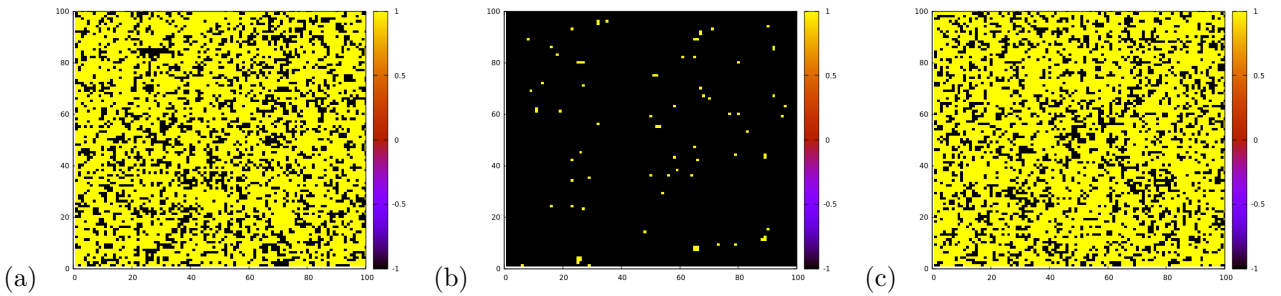


Figure 7: Morphology of (a) Top layer, (b) Mid layer and (c) Bottom layer for the ABA stacking ($J_{AA}/J_{BB} = 0.3$ and $J_{AB}/J_{BB} = -0.4$) at $T = 1.7$, (immediate higher neighbour than T_{comp}) with $M_t = -0.48$, $M_m = 0.98$, $M_b = -0.48$.

b. AAB composition

Reduced Residual Magnetisation (RRM):

The behaviour of RRM with the variation of antiferromagnetic and ferromagnetic coupling strength ratios (AFM and FM ratios, for brevity) [Fig.-9] leads us to predict their behaviours in the following way: The plots of RRM vs. AFM ratio [Fig.-10a], for a fixed FM ratio, predicts a functional relationship, $\Phi_1(J_{AA}/J_{BB}, J_{AB}/J_{BB})$, like:

$$\Phi_1(J_{AA}/J_{BB}, J_{AB}/J_{BB}) = a_1 \exp \left[-a_2 \left| \frac{J_{AB}}{J_{BB}} \right| \right] \quad (12)$$

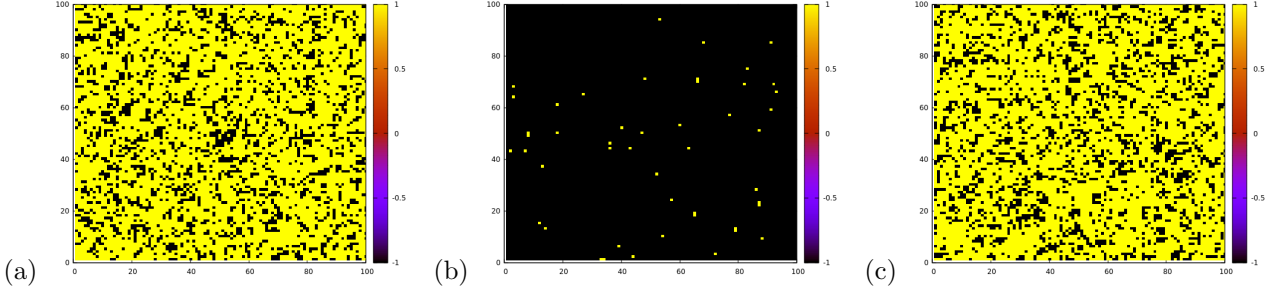


Figure 8: Morphology of (a) Top layer, (b) Mid layer and (c) Bottom layer for the ABA stacking ($J_{AA}/J_{BB} = 0.3$ and $J_{AB}/J_{BB} = -0.4$) at $T = 1.6$ (immediate lower neighbour than T_{comp}) with $M_t = -0.53$, $M_m = 0.99$, $M_b = -0.53$.

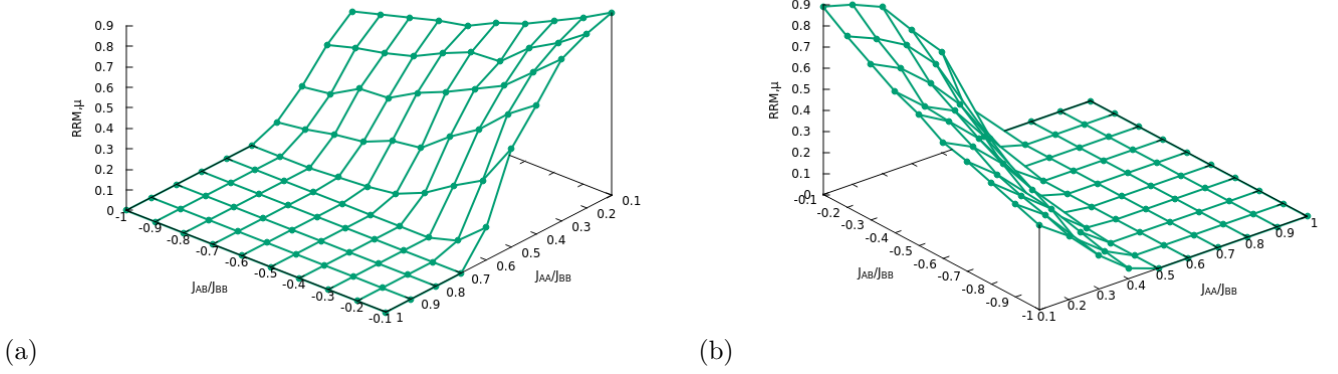


Figure 9: 3D plots of RRM vs. controlling factors for AAB configuration from two different angles of view.

where the coefficients a_1 and a_2 are functions of FM ratios i.e. $a_1 \equiv a_1(J_{AA}/J_{BB})$ and $a_2 \equiv a_2(J_{AA}/J_{BB})$ and Table 1 contains their variations.

J_{AA}/J_{BB}	0.1	0.2	0.3	0.4	0.5
a_1	0.966 ± 0.007	0.944 ± 0.016	0.940 ± 0.016	0.855 ± 0.027	0.818 ± 0.049
a_2	0.890 ± 0.014	1.166 ± 0.039	1.713 ± 0.045	2.662 ± 0.109	5.336 ± 0.344

Table 1: Variation of a_1 and a_2 with J_{AA}/J_{BB} , for AAB trilayer; the errors are standard asymptotic error for least square fitting

The plots of RRM vs. FM ratio [Fig.-10b], for fixed AFM ratios, predict a functional dependence, $\Phi_2(J_{AA}/J_{BB}, J_{AB}/J_{BB})$, like:

$$\Phi_2(J_{AA}/J_{BB}, J_{AB}/J_{BB}) = a_3 - a_4 \left(\frac{J_{AA}}{J_{BB}} \right)^2 \quad (13)$$

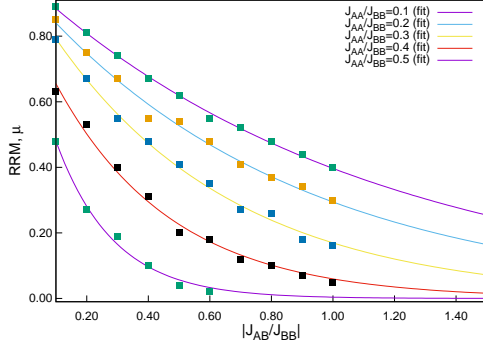
where the coefficients a_3 and a_4 are functions of J_{AB}/J_{BB} i.e. $a_3 \equiv a_3(J_{AB}/J_{BB})$ and $a_4 \equiv a_4(J_{AB}/J_{BB})$. Variations of a_3 and a_4 are listed in Table 2:

J_{AB}/J_{BB}	-0.1	-0.2	-0.3	-0.4	-0.5	-0.6	-0.7	-0.8	-0.9	-1.0
a_3	0.945 ± 0.027	0.852 ± 0.017	0.761 ± 0.003	0.674 ± 0.016	0.634 ± 0.020	0.562 ± 0.014	0.497 ± 0.016	0.487 ± 0.031	0.443 ± 0.030	0.401 ± 0.026
a_4	2.055 ± 0.138	2.241 ± 0.088	2.281 ± 0.022	2.289 ± 0.118	2.470 ± 0.140	2.241 ± 0.101	2.104 ± 0.241	2.461 ± 0.168	2.469 ± 0.320	2.314 ± 0.279

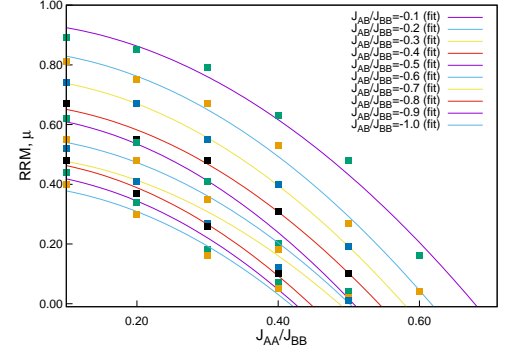
Table 2: Variation of a_3 and a_4 with J_{AB}/J_{BB} , for AAB trilayer; the errors are standard asymptotic errors for least square fitting

Temperature gap between Critical and Compensation temperatures, ΔT :

The behaviour of temperature gap between Critical and Compensation temperatures with the variation of AFM and FM ratios [Fig.-11], leads us to predict its behaviour in similar fashion as before.

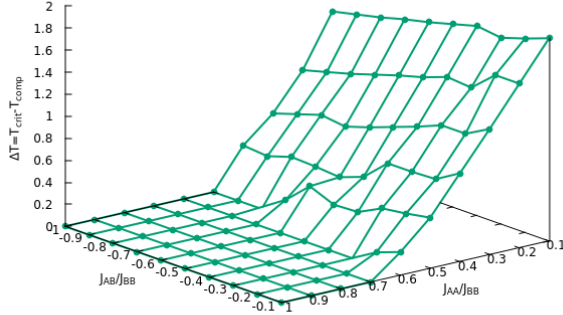


(a)

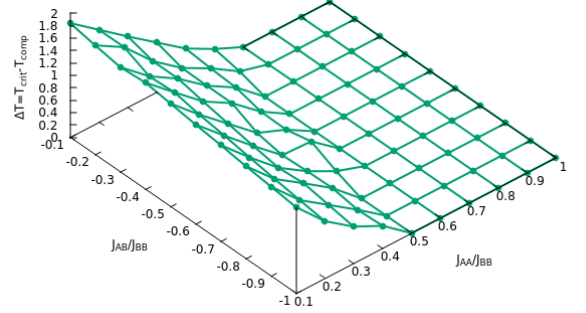


(b)

Figure 10: Plots of (a) Φ_1 vs. $\left| \frac{J_{AB}}{J_{BB}} \right|$ (b) Φ_2 vs. $\frac{J_{AA}}{J_{BB}}$ to show probable dependence of RRM of an AAB configuration.



(a)



(b)

Figure 11: 3D plots of $\Delta T = T_{crit} - T_{comp}$ vs. controlling factors for AAB configuration from two different angles of view.

The plots of ΔT vs. AFM ratio [Fig.-12a], for fixed FM ratios, predict a functional relationship, $\Psi_1(J_{AA}/J_{BB}, J_{AB}/J_{BB})$, like:

$$\Psi_1(J_{AA}/J_{BB}, J_{AB}/J_{BB}) = -a_5 \left| \frac{J_{AB}}{J_{BB}} \right| + a_6 \quad (14)$$

where the coefficients a_5 and a_6 are functions of FM ratios i.e. $a_5 \equiv a_5(J_{AA}/J_{BB})$ and $a_6 \equiv a_6(J_{AA}/J_{BB})$. Changes in the values of a_5 and a_6 are listed in Table 3:

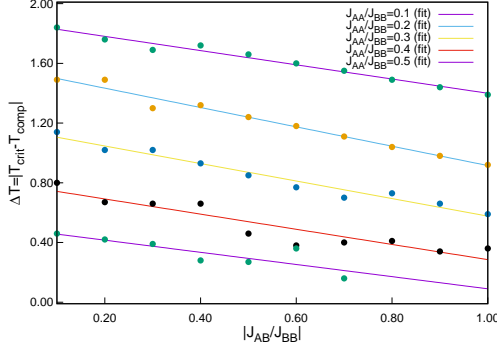
J_{AA}/J_{BB}	0.1	0.2	0.3	0.4	0.5
a_5	0.476 ± 0.026	0.648 ± 0.036	0.587 ± 0.039	0.508 ± 0.072	0.407 ± 0.113
a_6	1.876 ± 0.016	1.563 ± 0.022	1.164 ± 0.024	0.793 ± 0.044	0.497 ± 0.051

Table 3: Variation of a_5 and a_6 with FM ratio, for AAB trilayer; the errors are standard asymptotic error for least square fitting

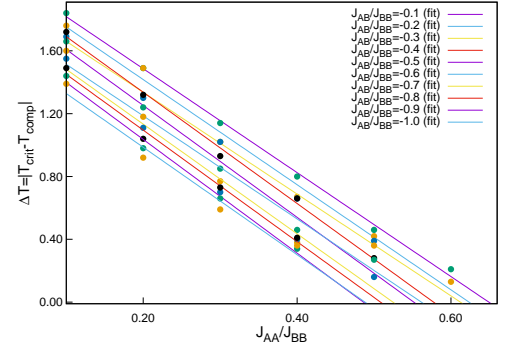
The plots of ΔT vs. FM ratio [Fig.-12b], for fixed AFM ratios, predict a functional dependence, $\Psi_2(J_{AA}/J_{BB}, J_{AB}/J_{BB})$, like:

$$\Psi_2(J_{AA}/J_{BB}, J_{AB}/J_{BB}) = -a_7 \left(\frac{J_{AA}}{J_{BB}} \right) + a_8 \quad (15)$$

where the coefficients a_7 and a_8 are functions of J_{AB}/J_{BB} i.e. $a_7 \equiv a_7(J_{AB}/J_{BB})$ and $a_8 \equiv a_8(J_{AB}/J_{BB})$. Variations of a_7 and a_8 are to be found in Table 4:



(a)



(b)

Figure 12: Plots of (a) Ψ_1 vs. $\left| \frac{J_{AB}}{J_{BB}} \right|$ (b) Ψ_2 vs. $\frac{J_{AA}}{J_{BB}}$ to show probable dependence of ΔT of an AAB configuration.

J_{AB}/J_{BB}	-0.1	-0.2	-0.3	-0.4	-0.5	-0.6	-0.7	-0.8	-0.9	-1.0
a_7	3.308 ± 0.082	3.346 ± 0.160	3.240 ± 0.111	3.540 ± 0.128	3.560 ± 0.250	3.280 ± 0.457	3.490 ± 0.251	3.550 ± 0.231	3.620 ± 0.242	3.420 ± 0.380
a_8	2.148 ± 0.032	2.086 ± 0.062	1.984 ± 0.037	2.044 ± 0.042	1.964 ± 0.083	1.842 ± 0.152	1.831 ± 0.083	1.805 ± 0.063	1.760 ± 0.066	1.670 ± 0.104

Table 4: Variation of a_7 and a_8 with AFM ratio, for AAB trilayer; the errors are standard asymptotic errors for least square fitting

c. ABA composition

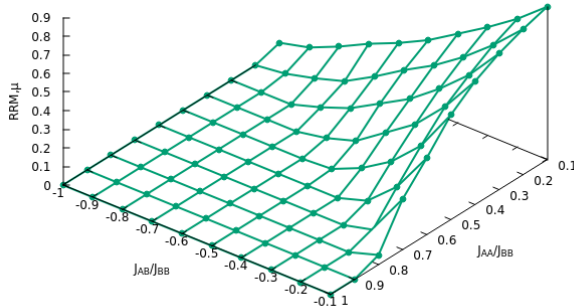
Reduced Residual Magnetisation (RRM):

Observing the trends from the plots of RRM [Fig.-13, Fig.-14a, Fig.-14b], for the ABA configuration, like the AAB configuration we predict two functional relationships like, $\Phi_3(J_{AA}/J_{BB}, J_{AB}/J_{BB})$ and $\Phi_4(J_{AA}/J_{BB}, J_{AB}/J_{BB})$ as:

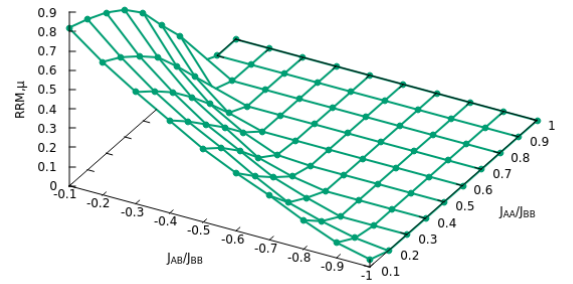
$$\Phi_3(J_{AA}/J_{BB}, J_{AB}/J_{BB}) = b_1 \exp \left[-b_2 \left(\frac{J_{AB}}{J_{BB}} \right)^2 \right] \quad (16)$$

$$\Phi_4(J_{AA}/J_{BB}, J_{AB}/J_{BB}) = b_3 - b_4 \left(\frac{J_{AA}}{J_{BB}} \right)^2 \quad (17)$$

where the coefficients b_1 and b_2 are functions of FM ratios i.e. $b_1 \equiv b_1(J_{AA}/J_{BB})$ and $b_2 \equiv b_2(J_{AA}/J_{BB})$ and their



(a)



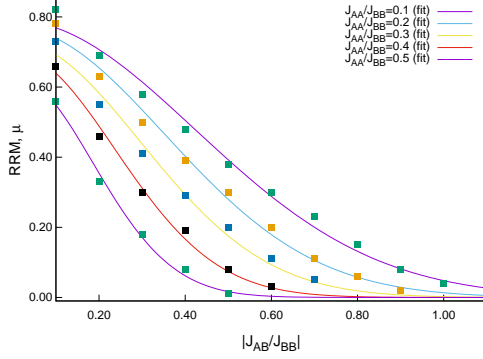
(b)

Figure 13: 3D plots of RRM vs. controlling factors for ABA configuration from two different angles of view.

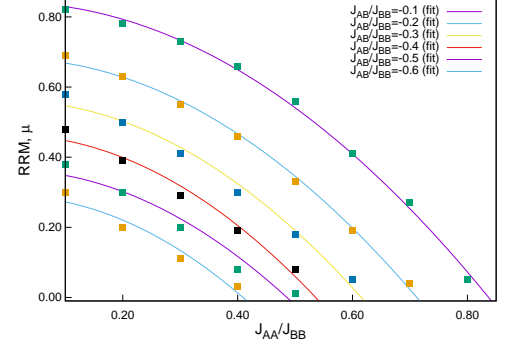
variations are in Table 5 and the coefficients b_3 and b_4 are functions of AFM ratios i.e. $b_3 \equiv b_3(J_{AB}/J_{BB})$ and $b_4 \equiv b_4(J_{AB}/J_{BB})$ and their variations are in Table 6.

J_{AA}/J_{BB}	0.1	0.2	0.3	0.4	0.5
b_1	0.791 ± 0.020	0.770 ± 0.020	0.733 ± 0.026	0.699 ± 0.024	0.635 ± 0.026
b_2	2.804 ± 0.155	4.048 ± 0.229	5.722 ± 0.430	8.972 ± 0.611	14.554 ± 1.14

Table 5: Variation of b_1 and b_2 with J_{AA}/J_{BB} , for ABA trilayer; the errors are standard asymptotic error for least square fitting



(a)



(b)

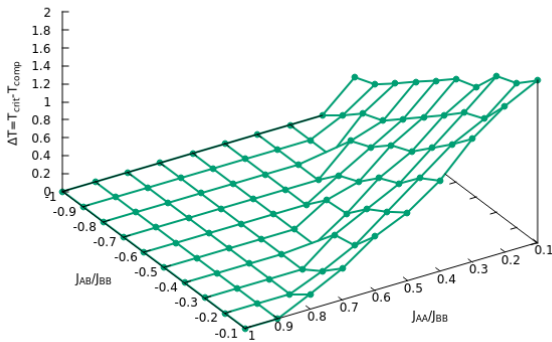
Figure 14: Plots of (a) Φ_3 vs. $\left| \frac{J_{AB}}{J_{BB}} \right|$ (b) Φ_4 vs. $\frac{J_{AA}}{J_{BB}}$ to show probable dependence of ΔT of an ABA configuration.

J_{AB}/J_{BB}	-0.1	-0.2	-0.3	-0.4	-0.5	-0.6
b_3	0.841 ± 0.009	0.682 ± 0.009	0.562 ± 0.017	0.464 ± 0.021	0.363 ± 0.026	0.290 ± 0.026
b_4	1.201 ± 0.027	1.345 ± 0.036	1.482 ± 0.086	1.615 ± 0.152	1.540 ± 0.189	1.729 ± 0.282

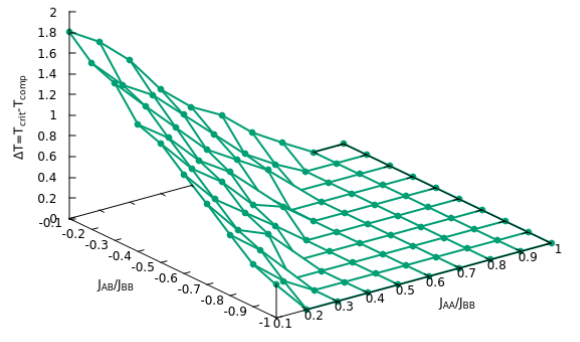
Table 6: Variation of b_3 and b_4 with J_{AB}/J_{BB} , for ABA trilayer; the errors are standard asymptotic error for least square fitting

Temperature gap between Critical and Compensation temperatures, ΔT :

The plots of ΔT [Fig.-15, Fig.-16a, Fig.-16b] may lead to functional relationships like:



(a)



(b)

Figure 15: 3D plots of ΔT vs. controlling factors for ABA configuration from two different angles of view.

$$\Psi_3(J_{AA}/J_{BB}, J_{AB}/J_{BB}) = -b_5 \left| \frac{J_{AB}}{J_{BB}} \right| + b_6 \quad (18)$$

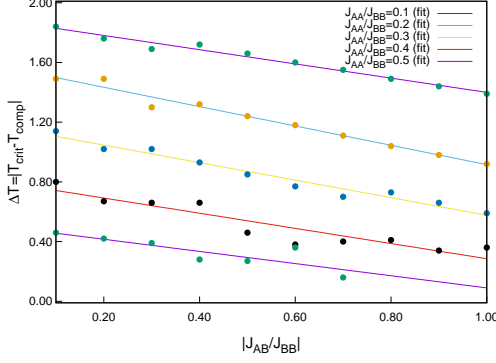
$$\Psi_4(J_{AA}/J_{BB}, J_{AB}/J_{BB}) = -b_7 \left(\frac{J_{AA}}{J_{BB}} \right) + b_8 \quad (19)$$

where $b_5 \equiv b_5(J_{AA}/J_{BB})$; $b_6 \equiv b_6(J_{AA}/J_{BB})$ and $b_7 \equiv b_7(J_{AB}/J_{BB})$; $b_8 \equiv b_8(J_{AB}/J_{BB})$.

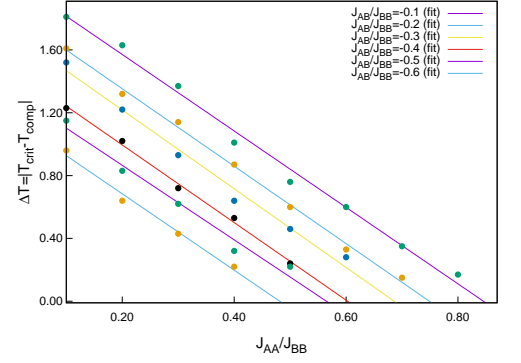
The obtained data of b_5 and b_6 , are in Table 7. Refer to Table 8 for the variations of b_7 and b_8 .

J_{AA}/J_{BB}	0.1	0.2	0.3	0.4	0.5
b_5	0.476 ± 0.026	0.648 ± 0.036	0.587 ± 0.039	0.508 ± 0.072	0.407 ± 0.113
b_6	1.876 ± 0.016	1.563 ± 0.022	1.164 ± 0.024	0.793 ± 0.045	0.497 ± 0.051

Table 7: Variation of b_5 and b_6 with J_{AA}/J_{BB} , for ABA trilayer; the errors are standard asymptotic error for least square fitting



(a)



(b)

Figure 16: Plots of (a) Ψ_3 vs. $\left| \frac{J_{AB}}{J_{BB}} \right|$ (b) Ψ_4 vs. $\frac{J_{AA}}{J_{BB}}$ to show probable dependence of ΔT of an ABA configuration.

J_{AB}/J_{BB}	-0.1	-0.2	-0.3	-0.4	-0.5	-0.6
b_7	2.433 ± 0.091	2.464 ± 0.059	2.506 ± 0.142	2.470 ± 0.093	2.370 ± 0.208	2.430 ± 0.190
b_8	2.056 ± 0.046	1.846 ± 0.026	1.719 ± 0.055	1.489 ± 0.031	1.339 ± 0.069	1.170 ± 0.052

Table 8: Variation of b_7 and b_8 with J_{AB}/J_{BB} , for ABA trilayer; the errors are standard asymptotic errors for least square fitting

V. Conclusion

a. AAB composition:

The zeroes of the function Ψ_2 lead us to the specific combinations of the coupling ratios for AAB composition Table 9 where the compensation ceases to exist within the ranges of our observation.

J_{AB}/J_{BB}	-0.1	-0.2	-0.3	-0.4	-0.5	-0.6	-0.7	-0.8	-0.9	-1.0
J_{AA}/J_{BB}	0.678	0.616	0.578	0.543	0.507	0.501	0.486	0.445	0.424	0.416
	± 0.008	± 0.014	± 0.017	± 0.021	± 0.024	± 0.024	± 0.038	± 0.025	± 0.035	± 0.034

Table 9: Table for maximum values of J_{AA}/J_{BB} for a fixed J_{AB}/J_{BB} for which the compensation effect just ceases, from the fitted formula of variation of RRM

Similarly We use zeroes of the function Ψ_2 to determine another set of specific combinations of the coupling ratios Table 10 for AAB configuration where the compensation just ceases to exist, from the data of temperature difference of T_{crit} and T_{comp} .

J_{AB}/J_{BB}	-0.1	-0.2	-0.3	-0.4	-0.5	-0.6	-0.7	-0.8	-0.9	-1.0
J_{AA}/J_{BB}	0.649	0.623	0.612	0.577	0.552	0.562	0.525	0.508	0.486	0.488
	± 0.019	± 0.035	± 0.024	± 0.024	± 0.045	± 0.091	± 0.045	± 0.038	± 0.037	± 0.062

Table 10: Maximum values of J_{AA}/J_{BB} for fixed J_{AB}/J_{BB} for which the compensation effect just ceases, from the fitted formula of Ψ_2

We can finally write the fitted formulae [Equation (20) and Equation (21)] for RRM (say, μ) and ΔT for AAB configuration as:

$$\left| \frac{M_{max,int}}{M_{sat}} \right| = \mu \left(\frac{J_{AA}}{J_{BB}}, \frac{J_{AB}}{J_{BB}} \right) = a_1 e^{-a_2 |J_{AB}/J_{BB}|} \left[a_3 - a_4 \left(\frac{J_{AA}}{J_{BB}} \right)^2 \right] \quad (20)$$

$$T_{crit} - T_{comp} = \Delta T \left(\frac{J_{AA}}{J_{BB}}, \frac{J_{AB}}{J_{BB}} \right) = \left[-a_5 \left| \frac{J_{AB}}{J_{BB}} \right| + a_6 \right] \left[-a_7 \left(\frac{J_{AA}}{J_{BB}} \right) + a_8 \right] \quad (21)$$

The coefficients $a_1, a_2, a_3, a_4, a_5, a_6, a_7$ and a_8 all are functions of $\frac{J_{AA}}{J_{BB}}$ and $\frac{J_{AB}}{J_{BB}}$.

b. ABA composition:

The zeroes of the function Φ_4 lead us to determine the specific combination of the coupling ratios from the RRM data for ABA composition where the compensation just ceases to exist (Ref. Table 11).

J_{AB}/J_{BB}	-0.1	-0.2	-0.3	-0.4	-0.5	-0.6
J_{AA}/J_{BB}	0.837 ± 0.010	0.712 ± 0.011	0.616 ± 0.020	0.536 ± 0.028	0.486 ± 0.035	0.410 ± 0.038

Table 11: Table for maximum values of J_{AA}/J_{BB} for a fixed J_{AB}/J_{BB} for which the compensation effect just ceases, from the fitted formula of variation of RRM

Similarly zeroes of Ψ_4 lead us to the combinations of the coupling ratios from the ΔT data for ABA composition where the compensation just ceases to exist (Ref. Table 12).

J_{AB}/J_{BB}	-0.1	-0.2	-0.3	-0.4	-0.5	-0.6
J_{AA}/J_{BB}	0.845 ± 0.037	0.749 ± 0.021	0.686 ± 0.045	0.603 ± 0.026	0.565 ± 0.058	0.481 ± 0.043

Table 12: Maximum values of J_{AA}/J_{BB} for a fixed J_{AB}/J_{BB} for which the compensation effect just ceases, from the fitted formula of variation of ΔT

We can finally write the fitted formulae [Equation (22) and Equation (23)] for RRM (say, μ) and ΔT for ABA configuration as:

$$\left| \frac{M_{max,int}}{M_{sat}} \right| = \mu \left(\frac{J_{AA}}{J_{BB}}, \frac{J_{AB}}{J_{BB}} \right) = b_1 e^{-b_2 (J_{AB}/J_{BB})^2} \left[b_3 - b_4 \left(\frac{J_{AA}}{J_{BB}} \right)^2 \right] \quad (22)$$

$$T_{crit} - T_{comp} = \Delta T \left(\frac{J_{AA}}{J_{BB}}, \frac{J_{AB}}{J_{BB}} \right) = \left[-b_5 \left| \frac{J_{AB}}{J_{BB}} \right| + b_6 \right] \left[-b_7 \left(\frac{J_{AA}}{J_{BB}} \right) + b_8 \right] \quad (23)$$

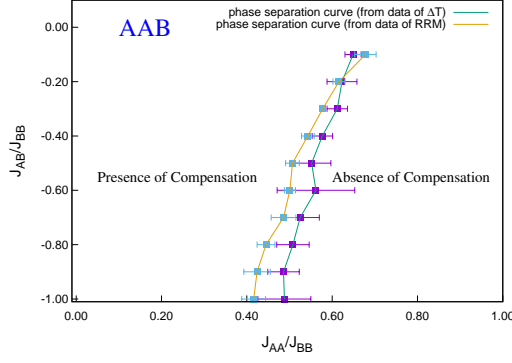
The coefficients $b_1, b_2, b_3, b_4, b_5, b_6, b_7$ and b_8 all are functions of $\frac{J_{AA}}{J_{BB}}$ and $\frac{J_{AB}}{J_{BB}}$.

Fig.-17 shows the phase separation curves obtained for two types of configurations under our valid ranges of observations which agree fairly well with [25] where the curves are obtained via MFA, EFA and MC simulations.

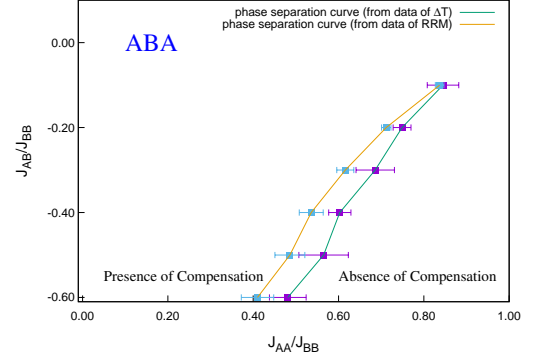
VI. Summary

Summarising, we have simulated magnetic and thermodynamic properties of a spin-1/2 Ising trilayer ferrimagnetic system on square lattice. For odd number of layers in layered ferrimagnets, neither site dilution nor mixed-spin cases are necessary for observing compensation on square trilayers. This type of systems is among the simplest layered ferrimagnetic systems for compensation. Each of the three layers of the system is made up of only one type of atoms, out of two i.e. A or B. The interactions between same type of atoms (A-A or B-B bonds) are ferromagnetic and between dissimilar atoms (A-B) is antiferromagnetic, resulting in two distinct configurations: A-A-B and A-B-A. The Hamiltonian, used in this article, is defined with the help of the Ising interactions. The system of both the configurations, at first, was initiated by randomly distributed equal number of up ($S = +1$) and down ($S = -1$) spins, mimicking a high temperature paramagnetic phase with no magnetic order. Then we decreased the temperature in steps of 0.1 till the final lowest temperature. Our objective is to find probable mathematical dependences of reduced residual magnetisation and absolute temperature differences between T_{crit} and T_{comp} , on relative interaction strengths in the Hamiltonian by analysing the system over a wide temperature range by MC single spin flip algorithm and hence obtain the phase diagram along with the lattice morphology. MC method is simpler to understand, takes fluctuations into account unlike MFA and yet produces accurate results. We have presented our results, analysed with the help of linear interpolation, and linear, quadratic and exponential curve fitting techniques.

Morphological studies are not common in similar works thus initially, we studied lattice morphologies at T_{crit} and in



(a)



(b)

Figure 17: Phase diagrams of (a) AAB and (b) ABA configurations from the fitted formulae; in both of the figures: rightside of the curves denote ferrimagnetic phase without compensation and left of the curves denote ferrimagnetic phase with compensation.

the neighbourhood of T_{comp} . The different spin density plots, of both the configurations, in those temperature regions [Fig.s 3-5 and Fig.s 6-8] reveal that T_{crit} and T_{comp} are fundamentally different. The formation of spin clusters, of different sizes, at T_{comp} is responsible for compensation phenomenon. We have also provided the values of sublattice magnetizations which show them vanishing at T_{crit} but at T_{comp} , non-zero values show the existence of magnetic ordering.

Next, for both AAB and ABA configurations, we present variations of reduced residual magnetisation and temperature gap between critical and compensation temperatures. We have two parameters in the Hamiltonian, namely, J_{AA}/J_{BB} and J_{AB}/J_{BB} in absence of an external magnetic field. We have varied J_{AA}/J_{BB} , from 0.1 to 1.0 and for each of the values J_{AB}/J_{BB} ranges from -0.1 to -1.0 . For each combination of them, we have obtained the values of reduced residual magnetisation and $(T_{crit} - T_{comp})$ from the plots like Fig. 2 and the 3D plots in Fig.s 9,11,13,15. Next we have proposed formulae for those mentioned quantities. The dynamics governed by these formulae leads to the phase diagrams (in the J_{AB}/J_{BB} - J_{AA}/J_{BB} plane) for both AAB [Fig. 17(a)] and ABA [Fig. 17(b)] type systems, which clearly divides the controlling parameter space into two regions: one with compensation and the other without compensation. In the phase diagrams where there is compensation, we clearly see that the range of J_{AA}/J_{BB} increases as $|J_{AB}/J_{BB}|$ gets smaller and the compensation happens only when $J_{AA} < J_{BB}$ which is in fair agreement with [25] and supports the findings in [24, 18, 19] for similar systems made up of antiferromagnetic and ferromagnetic bonds. We also notice that in the ABA configuration, the phase boundary is more inclined to the J_{AB}/J_{BB} axis than the AAB configuration. The ratio of ferromagnetic to antiferromagnetic bonds per site, in AAB configuration is 5:1 for the mid A-layer and 4:1 for the bottom B-layer compared to 2:1 in the mid B-layer and 4:1 in the bottom A-layer in ABA configuration. While in AAB, top A-layer has no antiferromagnetic bond, per site against a bond-ratio of 4:1 per site, in the top A-layer of ABA system. Greater number of antiferromagnetic bonds is responsible for the proneness to change of phase boundary with change in the values of J_{AB}/J_{BB} in ABA configuration.

If we have mathematical formulae, determining the presence and location of compensation points then they help technologists to choose materials according to their purpose without performing the wide range MC simulations themselves at precise parameter values. The layered magnetic materials, apt for compensation phenomenon, being economically cheap compared to rare-earth metals may become a strong candidate for the MCE. It would be interesting to study the behaviours of reduced residual magnetisation and the absolute difference in the critical and compensation temperatures in the case of mixed spin [58, 59] systems.

Acknowledgements

The authors acknowledge financial assistance provided by University Grants Commission, India and FRPDF grant of Presidency University, Kolkata, India. S.C. would like to extend his thanks to his senior Tamaghna Maitra for technical assistance.

References

1. Cullity B.D. and Graham C.D., *Introduction to Magnetic Materials*, **second ed.** (John Wiley & Sons, New Jersey, USA, 2008).

2. Connell G., Allen R. and Mansuripur M., J. Appl. Phys. **53** (1982) 7759.
3. Ostorero J., Escorne M. and Pecheron-Guegan A., Soulette F., Le Gall H., Journal of Applied Physics **75** (1994) 6103.
4. Camley R.E. and Barnaś J., Phys. Rev. Lett. **63** (1989) 664.
5. Phan M.H. and Yu S.C., J. Magn. Magn. Mater. **308** (2007) 325.
6. Ma S., Zhong Z., Wang D. et al., Eur. Phys. J. B **86** (2013) 133.
7. Herman M.A. and Sitter H., *Molecular Beam Epitaxy: Fundamentals and Current Status*, Vol. **7** (Springer Science & Business Media, 2012).
8. George S.M., Chem. Rev. **110** (2010) 111.
9. Stringfellow G.B., *Organometallic Vapor-Phase Epitaxy: Theory and Practice* (Academic Press, 1999).
10. Singh R.K. and Narayan J., Phys. Rev. B **41** (1990) 8843.
11. Stier M. and Nolting W., Phys. Rev. B **84** (2011) 094417.
12. Smits C.J.P., Filip A.T., Swagten H.J.M. et. al., Phys. Rev. B **69** (2004) 224410.
13. Chern G., Horng L. and Sheih W.K., Phys. Rev. B **63** (2001) 094421.
14. Sankowski P. and Kacmann P., Phys. Rev. B **71** (2005) 201303(R).
15. Godoy M. and Figueiredo W., Phys. Rev. E **61** (2000) 218.
16. Nakamura Y., Phys. Rev. B **62** (2000) 11742.
17. Godoy M., Leite V.S. and Figueiredo W., Phys. Rev. B **69** (2004) 054428.
18. Balcerzak T. and Szałowski K., Phys. A: Stat. Mech. Appl. **395** (2014) 183.
19. Szałowski K. and Balcerzak T., J. Phys.: Condensed Matter **26** (2014) 386003.
20. Szałowski K., Balcerzak T. and Bobak A., Journal of Magnetism and Magnetic Materials **323** (2011) 2095.
21. Diaz I.J.L. and Branco N.S., Phys. A Stat. Mech. Appl. **468** (2017) 158.
22. Diaz I.J.L. and Branco N.S., Phys. A Stat. Mech. Appl. **490** (2018) 904.
23. Santos J.P. and Barreto F.S., J. Magn. Magn. Mater. **439** (2017) 114.
24. Diaz I.J.L. and Branco N.S., Physica B **73** (2017) 529.
25. Diaz I.J.L. and Branco N.S., Physica A **540** (2019) 123014.
26. Laosiritaworn Y., Poulter J. and Staunton J.B., Phys. Rev. B **70** (2004) 104413.
27. Albano A.V. and Binder K., Phys. Rev. E **85** (2012) 061601.
28. Lubensky T.C. and Rubin M.H., Phys. Rev. B **12** (1975) 3885.
29. Kaneyoshi T., Physica A **293** (2001) 200.
30. Kaneyoshi T., Solid State Commun. **152**, (2012) 1686.
31. Kaneyoshi T., Physica B **407** (2012) 4358.
32. Kaneyoshi T., Phase Transitions **85**, (2012) 264.
33. Oitmaa J. and R.R.P. Singh, Phys. Rev. B **85** (2012) 014428.
34. Ohno K. and Okabe Y., Phys. Rev. B **39** (1989) 9764.
35. Benneman K.H., *Magnetic Properties of Low-Dimensional Systems* (Springer-Verlag, New York, 1986).
36. Albayrak E., Akkaya S. and Cengiz T., J. Magn. Magn. Mater. **321** (2009) 3726.
37. Balcerzak T. and Luźniak I., Physica A **388** (2009) 357.
38. Spichkin Y.I. and Tishin A.M., *The Magnetocaloric Effect and Its Applications* (Institute of Physics Publishing, Philadelphia, 2003).

39. Gschneidner K.A. Jr., Pecharsky V.K. and Tsokol A.O., Rep. Prog. Phys. **68** (2005) 1479 .
40. Warburg von E., Ann. Phys. **249(5)** (1881) 141.
41. Debye P., Ann. Phys. **386** (1926) 1154.
42. Giaque W.F., J. Am. Chem. Soc. **49** (1927) 1864.
43. Pecharsky V.K. and Gschneidner K.A. Jr., Phys. Rev. Lett. **78** (1997) 4494.
44. Tegus O., Brück E., Buschow K.H.J. and de Boer F.R., Nature **415** (2002) 150.
45. Provenzano V., Shapiro A.J. and Shull R.D., Nature **429** (2004) 853.
46. Xie Z.G., Geng D.Y. and Zhang Z.D., Appl. Phys. Lett. **97** (2010) 202504.
47. Sajid Sk. and Acharyya M., Phase Transitions **93** (2020) 62.
48. Chandra S. and Acharyya M., AIP Conference Proceedings **2220** (2020) 130037.
49. Fadil Z., Qajjour M., Mhirech A., Kabouchi B., Bahmad L. and Ousi Benomar W., Physica B **564** (2019) 104.
50. Fadil Z., Mhirech A. and Kabouchi B., Superlattice Microst. **134** (2019) 106224.
51. Fadil Z., Qajjour M. and Mhirech A., J Magn Magn Mater. **491** (2019) 165559.
52. Fadil Z., Mhirech A., Kabouchi B., Bahmad L. and Ousi Benomar W., Solid State Comm. **316–317** (2020) 113944.
53. Acharyya M., arXiv:2004.03930 (2020); DOI: doi.org/10.1016/j.spmi.2020.106648; To appear in Superlattices and Microstructures (Elsevier).
54. Landau D.P. and Binder K., *A guide to Monte Carlo simulations in Statistical Physics* (Cambridge University Press, New York, 2000).
55. Binder K. and Heermann D.W., *Monte Carlo simulation in Statistical Physics* (Springer, New York, 1997).
56. Metropolis N. et al., J. Chem Phys. **21** (1953) 1087.
57. Newman M.E.J. and Barkema G.T., *Monte Carlo methods in Statistical Physics* (Oxford University Press, New York, 1999)
58. Alzate-Cardona J.D., Barrero-Moreno M.C. and Restrepo-Parra E., J. Phys: Cond. Mat. **29** (2017) 445801.
59. Alzate-Cardona J.D., Sabogal-Suarez D. and Restrepo-Parra E., J. Magn. Magn. Mater. **429** (2017) 34.